J Mol Model (2012) 18:4191–4197
DOI 10.1007/s00894-012-1403-6

ORIGINAL PAPER

A rotary nano ion pump: a molecular dynamics study

A. Lohrasebi · M. Feshanjerdi

Received: 26 October 2011 / Accepted: 7 March 2012 / Published online: 27 April 2012

Abstract The dynamics of a rotary nano ion pump, inspired by the F_0 part of the F_0F_1-ATP synthase biomolecular motor, were investigated. This nanopump is composed of a rotor, which is constructed of two carbon nanotubes with benzene rings, and a stator, which is made of six graphene sheets. The molecular dynamics (MD) method was used to simulate the dynamics of the ion nanopump. When the rotor of the nanopump rotates mechanically, an ion gradient will be generated between the two sides of the nanopump. It is shown that the ion gradient generated by the nanopump is dependant on parameters such as the rotary frequency of the rotor, temperature and the amounts and locations of the positive and negative charges of the stator part of the nanopump. Also, an electrical potential difference is generated between the two sides of the pump as a result of its operation.

Keywords Nanopump · F_0-like motor · Ion gradient · Molecular dynamics

Introduction

Molecular motors are biological molecular machines that are powered by the hydrolysis of adenosine triphosphate (ATP) molecules and convert chemical energy into mechanical work. The resulting mechanical work is applied in all life processes of the cell, such as cell motility, intracellular transport, membrane transport and cell division. ATP molecules are produced by the rotary F_0F_1-ATP synthase (ATPase) protein motor [1–3]. This motor consists of two main parts. The first is the F_0 motor, which is embedded in the mitochondrial membrane. The second is the F_1 motor, which is located outside the membrane, and coupled via a shaft (the γ-shaft) to the F_0 part. The F_0 motor is thus constructed of a rotor part and a stator part. The rotor is a ring-shaped array of n identical sites, with a negative-charge associated with each site. The stator part contains two channels; one for entry of positive ions to the F_0 motor and the second for exiting of positive ions from the F_0 motor. Also, a positive-charge site is placed between the two channels. The flow of protons along an electrochemical gradient, between two side of the membrane, through the F_0 part of ATPase, causes rotation of the F_0 part and the γ-shaft transfers this rotation to the F_1 part in order to make ATP molecules from adenosine diphosphate (ADP) and phosphate (Pi). The motor can also work in reverse. The reverse rotation will be produced in the F_1 part by hydrolyzing ATP molecules to ADP and Pi. This rotation is transferred to the F_0 part which in turn produces an ion gradient. Therefore, the ATPase protein motor can produce an ion gradient by hydrolyzing ATP molecules.

Inspired by the F_0 part of this biological protein motor, we have designed an ion nanopump, composed of carbon nanotubes (CNTs) and graphite sheets, to produce an ion gradient. Carbon nanostructures such as CNTs are usually used to design nano-scale devices such as nanomotors, nanopumps and so on. Barreiro et al. [4] applied thermal gradients along a CNT to move a cargo along it. Also, Rurali et al. [5], Schoen et al. [6] and Shiomi et al. [7] suggested some other thermally driven linear nanomotors to transfer fullerene, gold nanoparticles and molecules of water through CNTs, respectively. Wang et al. [8] designed

A. Lohrasebi (✉) · M. Feshanjerdi
Department of Physics, University of Isfahan,
Isfahan, Iran
e-mail: lohrasebi@phys.ui.ac.ir

A. Lohrasebi
Department of Nano-Science,
Computational Physical Sciences Research Laboratory,
Institute of Research in Fundamental Sciences (IPM),
PO Box 19395–5531, Tehran, Iran

nanoscale propellers by using the CNT and, in another study, they suggested a rotary molecular motor driven by electron tunneling [9].

In another molecular dynamics (MD)-based study, a rotary nanomotor powered by the flow of ions was investigated [10]. Gong et al. designed a charge-driven molecular water pump by mimicking the biological ion channel [11]. In our previous work [12], we proposed a rotary nano-scale pump, constructed of CNTs and graphene blades, for the production of the density gradient that was also to be used for the separation of a mixture of two different gases, by using classical MD simulation. In this present work, we studied the dynamics of an F_0-like rotary nanopump, using both MD simulation [13], to simulate the dynamics of all the carbon atoms and the ions in the nanopump, and its stochastic variation [14], to simulate the motion of Na^+ ions in above and below the nanopump. The results show that the pump can generate an ion gradient when the rotor of the pump rotates mechanically. The paper is organized as follows. In the section on Atomistic structure and Computational details will introduce in Sec. 2. Section 3 contains the main results, including those for the produced ion gradient, the effect of temperature, the rotor frequency and the effect of stator charges on the generated ion gradient. A brief summary and conclusions are included in Sec. 4.

Atomistic structure and computational details

The structure of the proposed ion nanopump is shown schematically in Fig. 1. The ion nanopump is constructed of two main sections. The first section is the *rotor*, which is made of a (10,10) capped nanotube with a length of 23 Å and a (18,18) single wall carbon nanotube (SWCNT) of length 10 Å (Fig. 1a). The two coaxial nanotubes are connected together by 20 benzene rings. The space between the two SWCNTs is divided into ten identical sites by the rings. The components of the rotor are shown in Fig. 1a–d.

The second section of the ion nanopump is made of six graphene sheets (Fig. 1e,f), of the same area of 39×37.5 Å^2, with central circular cavities and two small holes in the upper and lower graphene sheets. The first small holes in the upper graphene sheet is shown by a solid (m) circle and the second small holes in the lower graphene sheet is shown by a dashed (n) circle in Fig. 1f. The rotor passes through the cavities. The radii of the holes are set at 10.5 Å in the upper and the lower graphene sheets, and for the rest of the holes at 16 Å. The radii of the two small holes in the upper and lower sheets are set at 4 Å and are centered on the perimeter of the upper and lower cavities. These small holes are used for ion transport, with one acting as the entrance channel and the other as the exit channel. A negative and a positive charge are attached to a carbon atom on the perimeter of the cavity in the second and fourth graphene sheets from the top, respectively (with strength ranging from 1*e* to 5*e*.). The negative charge is located near the entrance channel, and the positive charge is located near the exit channel. These are referred to as the *stator charges*, and are shown in Fig. 1e. As can be seen, the construction of our proposed nanopump is similar to the F_0 motor, but there are some differences between the structure of our nanopump and the F_0 motor. For example, the rotor of our nanopump has no charge, but a negative charge is located on the each site of the F_0 rotor. Also, the stator part of the F_0 motor has a positive charge between its two channels, but the stator of our nanopump has both a negative and a positive charge. The total number of carbon atoms in our system was 2,650, and the number the of Na^+ ions, which were located on the top of the pump, was 200. The particles are confined to a rectangular simulation box with dimensions of L_x=39, L_y= 37.5 and L_z=117 Å. Periodic boundary conditions are applied in the *x*- and *y*-directions, but not in the *z*-direction, because the Na^+ ions can just flow through the nanopump (from the upper side of the pump to the lower side).

Three types of interatomic potential are used in the simulations: the first generation Brenner potential [15] for modelling the covalent bonding between the carbon (C) atoms within the nanotubes, within the graphene sheets, and within the benzene rings. The Lennard-Jones(LJ) potential is used to describe the non-bonding interactions C–Na^+, Na^+–Na^+, and the C–C interactions in the nanotube–graphene, and graphene–graphene systems. The parameters of the LJ potential are ϵ_{Na+}=0.019044 eV, and σ_{Na+}=4.1 Å for the Na^+–Na^+ interaction in water [16], and ϵ_C=0.002413 eV and σ_C=3.4 Å for the C–C interaction [17]. The parameters for the C–Na^+ interaction are calculated using the Lorentz-Berthelot mixing rules, i.e., $\epsilon_{Na+C} = \sqrt{\epsilon_{Na+} \times \epsilon_C}$, and $\sigma_{Na+C} = 0.5(\sigma_{Na+} + \sigma_C)$.

The electrostatic interactions are modeled by the application of the reaction field (RF) method [18–20].

The dynamics of all carbon atoms are described by Newton's differential equation of motion, integrated via the application of the velocity Verlet method [13], with the integration time-step dt=1 fs. The motion of Na^+ ions in the water environment, above and below the nanopump, are modeled via the stochastic differential equation [10, 14]

$$m\frac{d^2r}{dt^2} = -\frac{dU}{dr} - \eta\frac{dr}{dt} + \Gamma_{rand}(t), \quad (1)$$

where the first term on the right hand side represents the deterministic force obtained from the sum of the potentials U, the second term represents the drag force, where η is the drag coefficient,

$$\eta = \frac{k_B T}{D}, \quad (2)$$

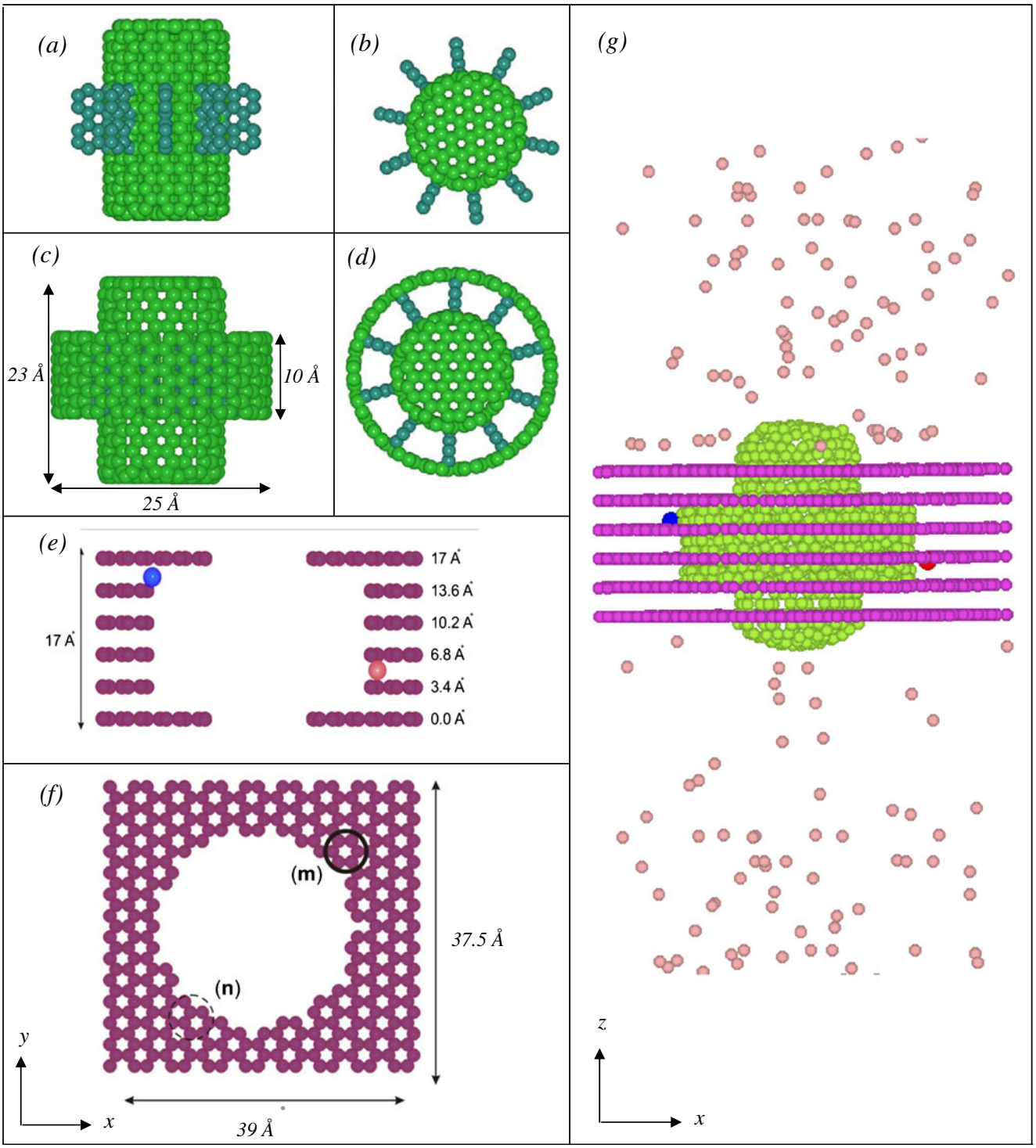

Fig. 1a–g The structure of nanopump components. **a**, **b** Side (**a**) and top (**b**) views of the 20 benzene rings that are connected to the (10,10) carbon nanotube (CNT). **c** Side view of the rotor, which is composed of two CNTs and 20 benzene rings that divide the rotor into ten equal parts. **d** Top view of the rotor. **e** Side view of the six graphene sheets. **f** Top view of the six graphene sheets. The entrance and the exit holes are shown by solid (*m*) and dashed (*n*) circles. **g** Complete structure of the nanopump in the equilibration state

where $D=0.29\times10^{-9}(m^2/s^{-1})$ [21] is the diffusion coefficient of Na^+ in the water, and the third term represents the stochastic, or the Brownian, force due to the randomly fluctuating water medium. The simulations are performed via our own FORTRAN-based code, considered a constant-NVT ensemble. The temperature is fixed by a conventional velocity-scaling approach [13].

Results and discussion

The system was equilibrated for 200 ps at a constant temperature without the presence of the ions, i.e., the nanopump and the collection of the positive ions were equilibrated independently without any interaction between them. Then, we forced the two tip rows of the carbon atoms in the rotor to rotate and hence induce a rotary motion for the whole rotor. At this time, the ions are transported through the channels (the entrance hole and the exit hole) that are embedded in the graphene sheets by entering the nanopump via the entrance hole and exiting the nanopump via the exit hole. The upper and lower graphene sheets also acted as boundaries separating the main part of the nanopump from the ion reservoirs.

The overall operation of the nanopump can be described as follows. A positive Na ion enters the entrance hole of the pump, due to sensing of the negative stator charge, and sits in the rotor site, which is located below the entrance channel. The rotation of the rotor causes the distancing of this ion from the entrance hole and its proximity to the exit hole. In this proximity the ion senses the positive stator charge; the resulting repulsion causes its exit toward the lower area of the pump. This process is repeated for a number of the other ions and thus, rotor rotation produces an ion gradient between both sides of the pump.

The ion concentration in the lower (C_1) and upper (C_2) sides of the nanopump are the same at the beginning of the simulations, and are equal to 2.5 mol/l. In the first simulation, the negative and positive stator charges are set at $-4e$ and $+4e$, respectively. The temperature and rotor frequency are set at T=300 and f=10^{12} Hz, respectively. Following the equilibration phase, the nanopump is simulated for a period of 10 ns. After 10 ns, the ion concentrations in the upper and lower sides of the nanopump are equal to 2 and 2.95 mol/l, respectively. The ratio of the ion concentration in the lower side to that of the upper side of the pump, is C_1/C_2=1.46. The simulation snapshot corresponding to the state of the nanopump at the conclusion of the simulation phase is shown in Fig. 1g.

Figure 2 shows the variation in the ratio of C_1 to C_2 as a function of the rotational frequency of the rotor of the pump. As can be seen from this figure, when the rotor rotational frequency increases, the ratio of C_1/C_2 also increases, up to a frequency equal to 10^{12} Hz. At greater rotor rotational frequencies, the ratio of C_1/C_2 will decrease with increase in rotor frequency, because, when the rotor frequency increases, the amount of time the ions have to situate themselves on the rotor sites, and consequently the probability of the ions entering the pump, will decrease and therefore the above mentioned ratio will fall.

In order to investigate the effect of temperature on ion pumping, some simulations were performed under conditions in which the negative and positive stator charges are set at $-4e$ and $+4e$, respectively. Figure 3 shows the effect of temperature on the ability of the nanopump to produce the ion gradient, at frequencies of 5×10^{11}, 10^{12} and 5×10^{12} Hz. For each frequency, it was observed that the ratio of C_1/C_2 increases with increasing temperature and then reaches its maximum value at the specific temperature. However, the ability of the pump to produce the ion gradient is decreased for higher temperatures. For example, the ratio of C_1/C_2 reaches its maximum value at T=600 K, and then decreases for temperatures larger than T=600 K. Also, it can be seen that the specific temperature increases for higher frequency of the pump (at the specific temperature, the pump has a maximum ability to produce the ion gradient.). For instance, the specific temperature for the pump frequency of f=5×10^{11} Hz is 500 K, While the specific temperatures is 700 K for the pump frequency of f=5×10^{12} Hz.

To ascertain the influence of the amounts of stator charges on the ability of the pump to produce the ion

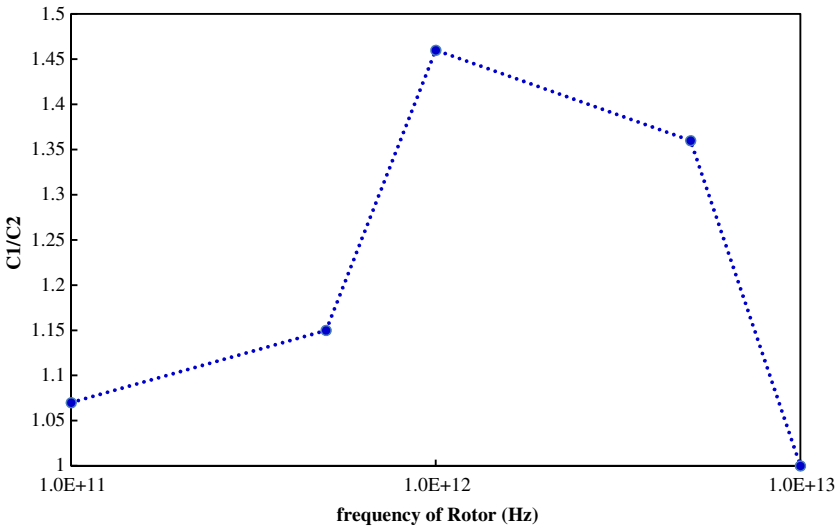

Fig. 2 Variations in ratio of C_1 to C_2 as a function of rotor rotational frequency of the pump. The ion density is set at 2.5 mol/l and the negative and positive stator charges are set at $-4e$ and $+4e$, respectively; T=300 K

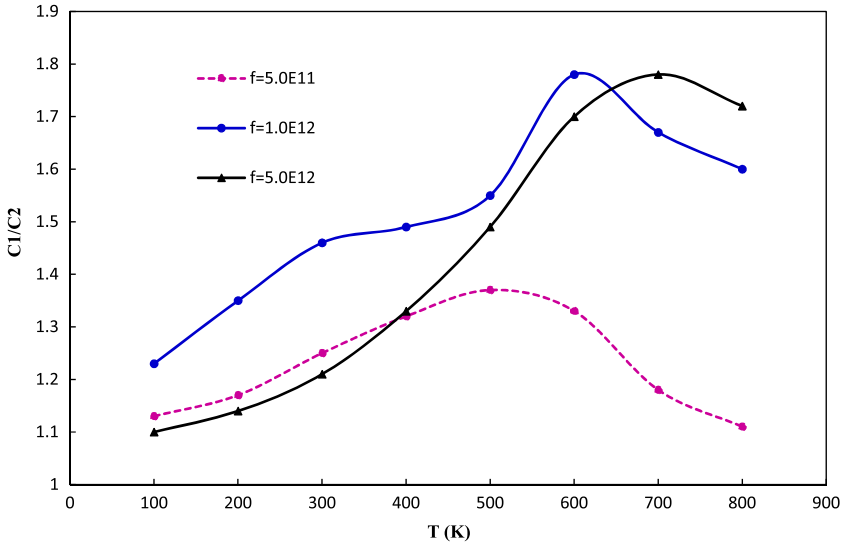

Fig. 3 Variations in the ratio of C_1 to C_2 as a function of temperature for $f=5\times10^{11}$, 10^{12} and 5×10^{12} Hz. The ion density is set at 2.5 mol/l and the negative and positive stator charges are set at $-4e$ and $+4e$, respectively

gradient(at $T=300$ and $f=10^{12}$ Hz), we performed some simulations by setting the stator charge strength in a range between $1e$ to $5e$. Figure 4 shows the variations in the ratio of C_1/C_2 as a function of the amount of the stator charges. It can be seen that when the stator charge increases, C_1/C_2 also increases, up to a point, i.e., the transferring rate of ions rises upon increasing the charges on the stator. However, when the amount of the stator charge reaches $3e$, the ability of the pump to produce the ion gradient begins to decline. This behavior is due to the fact that, when the stator charges are increased to $4e$ or $5e$, the electrostatic force between the ions and the positive stator charge becomes large and, hence, the repulsive force between the ions and positive stator charge pushes the ions away from the exit hole of the pump and, as a result, the rotor sites will not be empty and therefore other ions cannot enter and sit in the rotor sites. Therefore, the ion transport rate is reduced and this corresponds with a decrease in the C_1/C_2 ratio.

Next, we examined the role of the locations of stator charges on the ability of the pump to produce the ion gradient. In the MD simulations, the locations of the stator charges were varied in two ways: the first was that they were moved from one graphene sheet to another in the opposite direction (case I), i.e., they were moved vertically. The second was that the negative charge was fixed and the positive charge moved from one graphene sheet to another (case II). Figure 5a shows the variations in the ratio C_1/C_2 with the change in location of the stator charges for case I (at $T=300$ K and frequency equal to 10^{12} Hz). The stator charges were set at $-4e$ and $+4e$ for the negative and positive stator charges, respectively. From this figure it can be seen that when the negative and the positive stator charges are positioned on the second and fourth graphene sheets, respectively, the C_1/C_2 has a maximum value, and when both are positioned on the third graphene sheet, C_1/C_2 has a minimum value. Figure 5b shows how the C_1/C_2 ratio changes when the location of the negative charge is fixed on

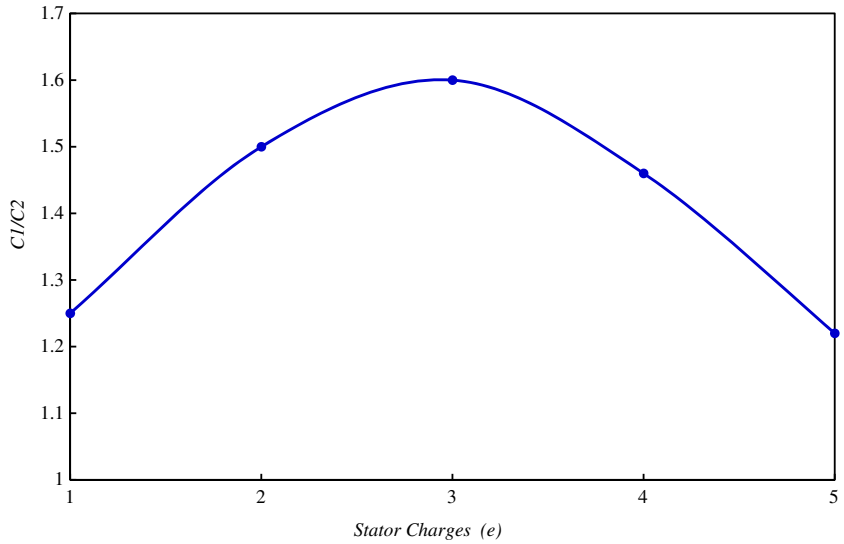

Fig. 4 Variation in the C_1/C_2 ratio as a function of the amount of stator charges. The temperature and rotor frequency are set at $T=300$ K and $f=10^{12}$ Hz, respectively

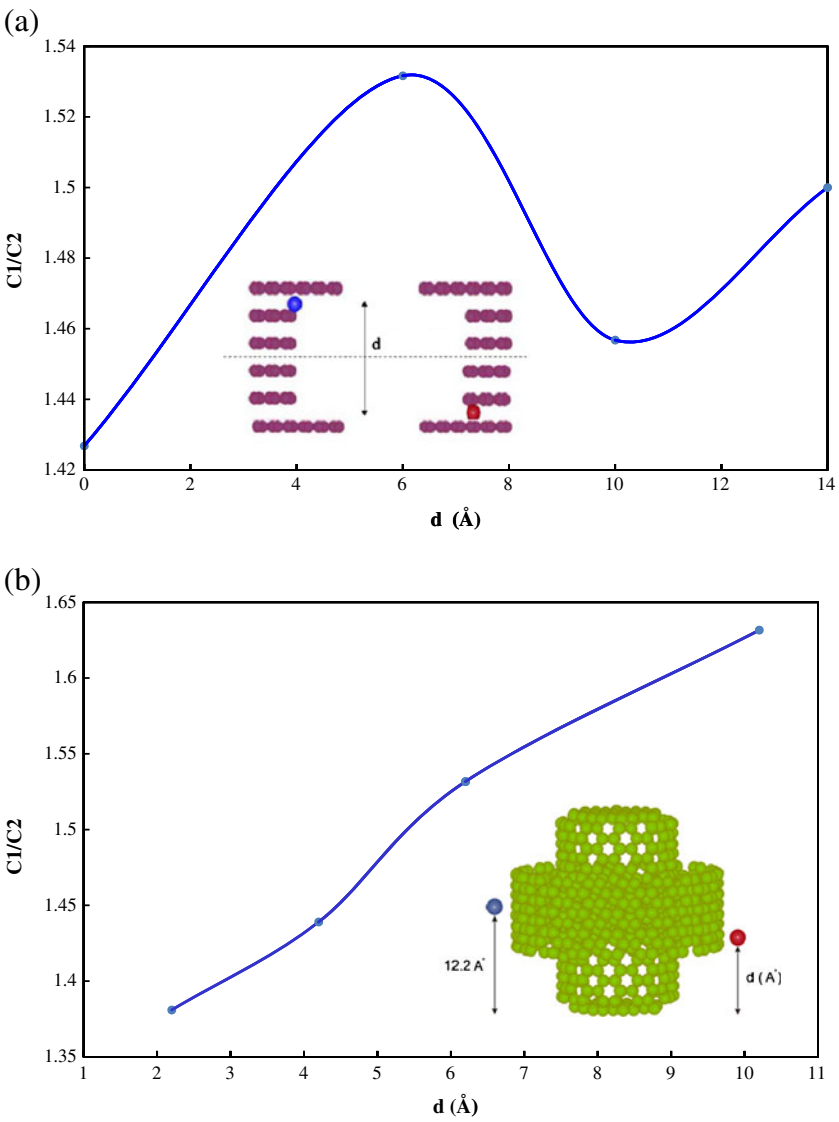

Fig. 5a,b Effect of change in locations of the stator charges on the ability of the pump to produce an ion gradient. The ion density is set at 2.5 mol/l and the negative and positive stator charges are set at $-4e$ and $+4e$, respectively; T=300 K and f=10^{12} Hz. **a** Variations in C_1/C_2 ratio with change in location of stator charges for case I. When the negative and positive stator charges are positioned on the second and fourth graphene sheets, respectively, the C_1/C_2 has a maximum value. **b** Variations in the ratio of C_1/C_2 with the change in locations of stator charges for case II

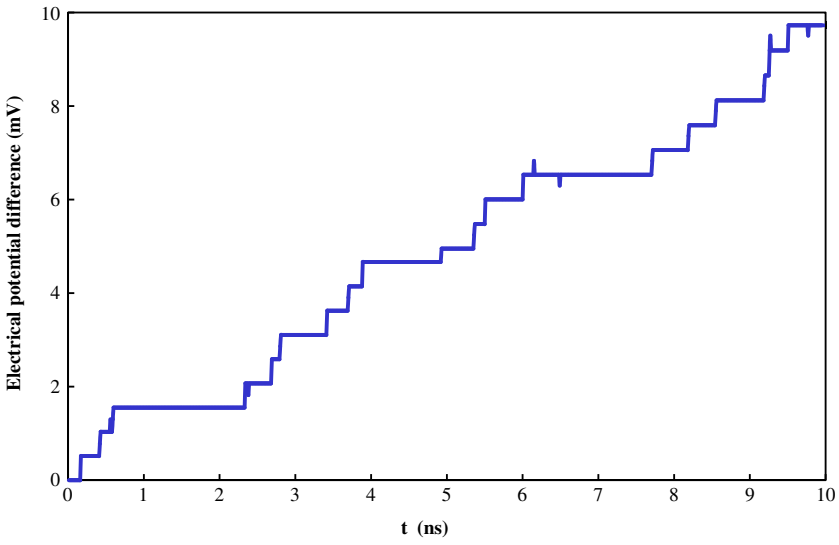

Fig. 6 Variations in the electrical potential difference between the two sides of the pump as a function of simulation time. The ion density is set at 2.5 mol/l and the negative and positive stator charges are set at $-4e$ and $+4e$, respectively; T=300 K and f=10^{12} Hz

the second graphene sheet and the positive charge moves from one graphene sheet to another (case II). Finally, we calculated the electrical potential difference between the two sides of the pump due to ion transfer from the upper side to the lower side of the pump by using the Nerst equation shown below:

$$\Delta V = \frac{RT}{zF} \log\left(\frac{C_1}{C_2}\right) \quad (3)$$

where R corresponds to the gas constant, T is the temperature, z is the valance of ion and F refers to the Faraday constant.

Figure 6 shows the potential difference between the two sides of the pump with the passage of time, during the entire course of the simulation. As can be seen from this figure, the potential difference between the pump sides increases when the ions move from the upper side to the lower side and is about 10 mV after 10 ns.

Conclusions

This paper provides the outline of a mechanical rotary ion nano-scale pump, mimicking the mechanism of the rotary motion of the F_0 part of an F_0F_1 ATPase bio-nanopump. Deterministic and stochastic MD simulations, based on many-body and two-body interatomic potentials, were employed to model the dynamics of such a nanopump and to examine the influence of environmental parameters, such as temperature, on the dynamics. It was found that this pump can produce an ion gradient along its two sides. Also, we observed that ion gradient generation is affected by the rotational frequency of the pump. Furthermore, our simulations show that we can use stator charges as parameters to control the operation of such a pump. This pump can also be used to produce the electrical potential difference between the pump sides, as does the F_0F_1 ATPase bio-nanopump.

References

1. Xing J, Wang H, Ballmoos CV, Dimroth P, Oster G (2004) Torque generation by the F_0 motor of the sodium ATPase. Biophys J 87:21482163
2. Aksimentiev A, Balabin IA, Fillingame RH, Schulten K (2004) Insights into the molecular mechanism of rotation in the F_0 sector of ATP synthase. Biophys J 86:1332–1344
3. Lohrasebi A, Jamali Y, Rafii-Tabar H (2008) Modeling the effect of external electric field and current on the stochastic dynamics of ATPase nano-biomolecular motors. Phys A 387:5466–5476
4. Barreiro A, Rurali R, Hernndez ER, Moser J, Pichler T, Forr L, Bachtold A (2008) Sub-nanometer motion of cargoes driven by thermal gradients along carbon nanotubes. Science 320:775–778
5. Rurali R, Hernandez ER (2010) Thermally induced directed motion of fullerene clusters encapsulated in carbon nanotubes. Chem Phys Lett 497:62–65
6. Schoen PAE, Walther JH, Arcidiacono S, Poulikakos D, Koumoutsakos P (2006) Nanoparticle traffic on helical tracks: Thermophoretic mass transport through carbon nanotubes. Nano Lett 6:1910–1917
7. Shiomi J, Maruyama S (2009) Water transport inside a single-walled carbon nanotube driven by a temperature gradient. Nanotechnology 20(055708):1–5
8. Wang BY, Kral P (2007) Chemically tunable nanoscale propellers of liquids. Phys Rev Lett 98(266102):1–4
9. Wang B, Vukovic L, Kral P (2008) Nanoscale rotary motors driven by electron tunneling. Phys Rev Lett 101:1868081–1868084
10. Lohrasebi A, Rafii-Tabar H (2008) Computational modeling of an ion-driven nanopump. J Mol Graph Model 29:1025–1029
11. Gong X, Ji L, Lu H, Wan R, Li J, Hu J, Fang H (2007) A charge-driven molecular water pump. Nature 2:709712
12. Lohrasebi A, Jamali Y (2011) Computational modeling of a rotary nanopump. J Mol Graph Model 27:116–123
13. Allen MP, Tildesley DJ (1987) Computer simulation of liquids. Clarendon, Oxford
14. Wang H (2003) Mathematical theory of molecular motors and a new approach for uncovering motor mechanism. IEE Proc Nanobiotechnol 150:127–133
15. Brenner DW (1990) Empirical potential for hydrocarbons for use in simulating the chemical vapor deposition of diamond films. Phys Rev B 42(9458):1–14
16. Crozier PS, Henderson D, Rowley RL, Busath DD (2001) Model channel ion currents in NaCl-SPC/E solution with applied-field molecular dynamics. Biophys J 81:3077–3089
17. Stan G, Bojan MJ, Curtarolo S, Gatica SM, Cole MW (2000) Uptake of gases in bundles of carbon nanotubes. Phys Rev B 62:2173–2180
18. Neumann M (1985) The dielectric constant of water. Computer simulations with the MCY potential. J Chem Phys 82:5663–5672
19. Tironi IG, Sperb R, Smith PE, van Gunsteren WF (1995) A generalized reaction field method for molecular dynamics simulations. J Chem Phys 102:5451–5459
20. Praprotnik M, Janezic D, Mavri J (2004) Temperature dependence of water vibrational spectrum: a molecular dynamics simulation study. J Phys Chem A 108:1105611062
21. Charron FM, Blanchard MG, Lapointe JY (2006) Intracellular hypertonicity is responsible for water flux associated with Na+/glucose cotransport. Biophys J 90:3546–3554